MRST-Shale: An Open-Source Framework for Generic Numerical Modeling of Unconventional Shale and Tight Gas Reservoirs

Bin Wang[1]

1. Craft and Hawkins Department of Petroleum Engineering, Louisiana State University; bwang31@lsu.edu

Highlights

- A generic numerical model for shale gas flow in tight reservoir is proposed
- A flexible open-source framework OpenShale is developed with EDFM
- EDFM can lead to large error for shale gas flow without help of grid refinement
- A new geomechanics model for hydraulic and natural fractures is proposed and evaluated
- OpenShale successfully applied in field history matching and new model evaluation

Abstract

We present a generic and open-source framework for the numerical modeling of the expected transport and storage mechanisms in unconventional gas reservoirs. These unconventional reservoirs typically contain natural fractures at multiple scales. Considering the importance of these fractures in shale gas production, we perform a rigorous study on the accuracy of different fracture models. The framework is validated against an industrial simulator and is used to perform a history-matching study on the Barnett shale. This work presents an open-source code that leverages cutting-edge numerical modeling capabilities like automatic differentiation, stochastic fracture modeling, multi-continuum modeling and other explicit and discrete fracture models. We modified the conventional mass balance equation to account for the physical mechanisms that are unique to organic-rich source rocks. Some of these include the use of an adsorption isotherm, a dynamic permeability-correction function, and an embedded discrete fracture model (EDFM) with fracture-well connectivity. We explore the accuracy of the EDFM for modeling hydraulically-fractured shale-gas wells, which could be connected to natural fractures of finite or infinite conductivity, and could deform during production. Simulation results indicates that although the EDFM provides a computationally efficient model for describing flow in natural and hydraulic fractures, it could be inaccurate under these three conditions: 1. when the fracture conductivity is very low. 2. when the fractures are not orthogonal to the underlying Cartesian grid blocks, and 3. when sharp pressure drops occur in large grid blocks with insufficient mesh refinement. Each of these results are very significant considering that most of the fluids in these ultra-low matrix permeability reservoirs get produced through the interconnected natural fractures, which are expected to have very low fracture conductivities. We also expect sharp pressure drops near the fractures in these shale gas reservoirs, and it is very unrealistic to expect the hydraulic fractures or complex fracture networks to be orthogonal to any structured grid. In conclusion, this paper presents

 doi:10.20944/preprints202001.0080.v1

an open-source numerical framework to facilitate the modeling of the expected physical mechanisms in shale-gas reservoirs. The code was validated against published results and a commercial simulator. We also performed a history-matching study on a naturally-fractured Barnett shale-gas well considering adsorption, gas slippage & diffusion and fracture closure as well as proppant embedment, using the framework presented. This work provides the first open-source code that can be used to facilitate the modeling and optimization of fractured shale-gas reservoirs. To provide the numerical flexibility to accurately model stochastic natural fractures that are connected to hydraulically-fractured wells, it is built atop other related open-source codes. We also present the first rigorous study on the accuracy of using EDFM to model both hydraulic fractures and natural fractures that may or may not be interconnected.

Source code is available at https://github.com/BinWang0213/MRST_Shale

Key words: shale gas; MRST; embedded discrete fracture model; open-source implementation

1 Introduction

Unconventional gas resources gain great interest recently due to successful economic development and strong energy supply around the world. Advancement of horizontal well drilling and hydraulic fracturing technology as well as better understanding unconventional reservoirs drives substantial growth of shale gas production (Bowker, 2007). Unlike conventional reservoirs, unconventional shale gas reservoirs can be characterized by ultra-low permeability, low porosity, complex transport mechanism and multi-scale fractures (Akkutlu et al, 2018). Development of unconventional resources is more technology-demanding and expensive. Thus, accurate modeling and numerical simulation of shale gas flow is critical for evaluating, designing and managing stimulation and production processes.

Well-established flow and transport theory for conventional reservoir rocks are not directly applicable to unconventional porous media (Gensterblum et al, 2015). For decades, researchers have been investigating the storage and transport mechanisms for unconventional reservoirs, which includes gas desorption, adsorbed gas porosity, gas slippage, and Knudsen diffusion, etc (Javadpour et al, 2007; Wang and Reed, 2009; Civan et al, 2010,2011; Sakhaee and Bryant, 2012; Akkutlu and Fathi, 2012, Yu et al, 2016 and Tan et al, 2018). In addition, the fractured shale matrix is comprised of a hierarchical network of pores down to a few nanometers, cracks and micro-fractures, which makes the formation a multi-scale porous medium with large heterogeneity and anisotropy (Akkutlu et al, 2018). Hence, the complex gas transport mechanisms and multiscale fracture system (**Figs. 1-2**) pose a great challenge to accurately and efficiently evaluate and simulate well performance in shale gas reservoirs.

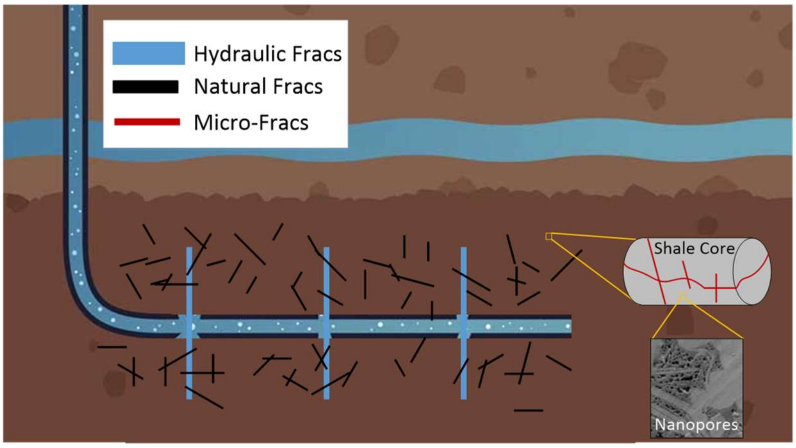

Fig 1 – Multi-scale natural of shale gas production

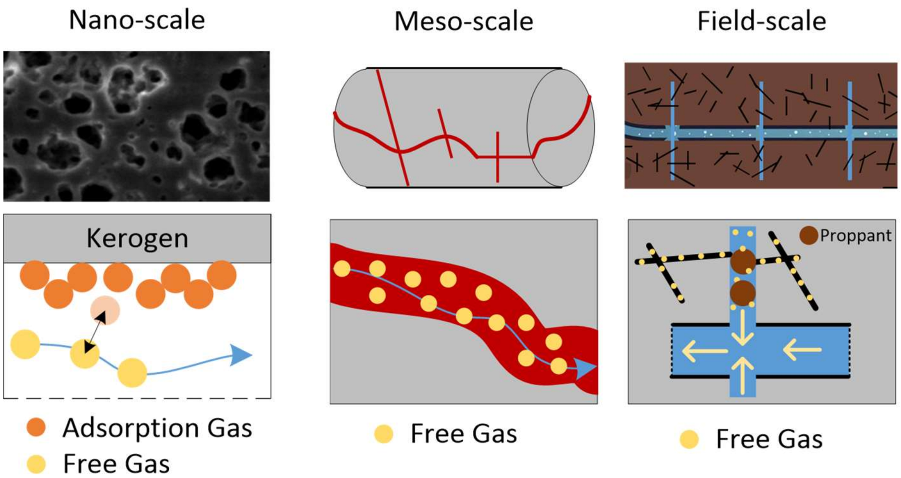

Fig 2 – Multi-scale shale gas storage and transport

In recent years, significant efforts have been made to model gas flow in unconventional reservoirs. These methods can be categorized into analytical model, semi-analytical model and numerical simulations. The analytical method dates back to 1970s, where the line-source fundamental solution is derived for simple fracture geometry such as single bi-wing hydraulic fractures and pseudo-pressure is applied to linearized the non-linear real gas equation (Gringarten et al, 1974, Cinco et al, 1978 and Agarwal 1979). Recently, the analytical method is extended into semi-analytical method to consider complex fracture networks and shale gas storage mechanism based on the boundary element method (Zuo et al, 2016, Chen et al, 2015, 2016, 2017, 2018; Yang et al, 2016a, 2016b, 2017, Yu et al, 2016b, 2017 and Li et al, 2018). Although analytical-based method is fast and accurate, it is difficult to handle rock heterogeneity, multi-phase, multi-compositional and strong non-linear transport mechanisms in shale gas flow problems (Houze et al, 2010 and Olorode et al, 2013). On the other hand, numerical simulation has been proven to be is the most general and rigorous method to account for arbitrary non-linear physics and fracture geometry for unconventional reservoirs (Olorode et al, 2013,2017 and Cipolla et al, 2012). Highly coupled non-linear physics and treatment of multi-scale fractured system are two key issues in shale gas flow simulation. Fully implicit scheme with Automatic Differentiation (AD) is a robust and generic method to solve the highly coupled non-linear problem accurately and efficiently (Zhou et al, 2011 and Krogstad et al, 2015). In terms of multi-scale fractured system, dual continuum method (Warren and Root, 1963) and discrete fracture method (Karimi-fard et al, 2004, Hoteit and Firoozabadi, 2005, Hajibeygi et al, 2011 and Moinfar et al, 2014) are generally used to model highly connected fractures and long, disconnected hydraulic/natural fractures (Fig. 1), respectively. A hierarchical method is also proposed by integrating continuum method and discrete fracture method for multi-scale fractured system where the micro-fractures are upscaled into matrix permeability tensor and hydraulic/natural fractures are modeled explicitly (Lee et al, 2001and Karimi-Fard et al, 2006). Unstructured gridding with local grid refinement (LGR) is generally used to capture the irregular fracture geometry and sharp pressure gradient near the fractures. However, it is are still challenging to generate conforming mesh efficiently for complex fracture networks (Karimi-Fard, Durlofsky, 2016). Recently, an embedded discrete fracture model is developed to resolve the complex gridding issue. Using EDFM, the complex fractures are embedded in conventional matrix grids without conforming the matrix grids with fracture plane, thus it is more efficient for complex fracture networks. In addition, it can be easily integrated into well-established reservoir simulator without accessing the code (Xu, 2015 and Olorode et al, 2017). **Table 1** shows the advantages and disadvantages of these method where unstructured grid and EDFM are the two most promising methods for generic shale gas simulation with multi-scale fractures.

Table 1. Comparison of shale gas flow simulation methods

	Analytical	Semi-analytical	Structured grid	Unstructured grid	EDFM
Accuracy	++	++	+++	+++	++
Nonlinear mechanisms*	+	+	+++	+++	+++
Rock heterogeneity	+	+	+++	+++	+++
Fracture gridding	+++	+++	+	+	+++
Preprocessing** efficiency	+++	+++	+++	+++	++
Computational*** efficiency	+++	+++	+	++	++

* Nonlinear gas transport & storage model, multi-phase flow, compositional flow

** 2D/3D geometry calculations, such plane-plane intersection, point-plane distance

*** linear algebra and Newton's calculations

Flow and transport theory and models for unconventional reservoir is a rapid evolving area of research, many of the existing and newly discovered phenomenon have not been completely understood. Also, the effect of these mechanism on practical well performance is not clear. To the best of our knowledge, almost all existing numerical models for shale gas reservoir are implemented in in-house simulators or commercial simulators (Jiang and Younis, 2015, Cao et al, 2016, Xu et al, 2017, Wang et al, 2017 and Akkutlu et al, 2018). Hence, it is necessary to develop a flexible and generic open-source framework to fill this gap.

In this paper, a generic numerical model is developed to simulate shale gas flow in unconventional reservoirs with multi-scaled fractures, which can be used to integrate any shale gas transport and storage mechanism for unconventional reservoirs as well as the geomechanics effect for fracture system. An efficient and flexible framework (OpenShale) is also developed using an open-source reservoir simulation toolkit (MRST) and EDFM. OpenShale can handle deterministic hydraulic fractures and stochastic natural fractures with arbitrary geometry and distribution. The framework is firstly verified against a commercial simulator and an in-house reservoir simulator that employs unstructured grid to simulate shale gas transport with non-planar hydraulic fracture, gas desorption, gas slippage & diffusion. The advantages and limitation of EDFM for shale gas flow problem is also discussed. Finally, field application of history matching and new geomechanics model evaluation are studied.

2 Mathematical equations

Considering the isothermal single-component single-phase gas flow in 2D fractured porous media with 1D fracture line without gravity effect. The general governing equation for shale gas flow in matrix (Ω_m), considering storage (m_{ad}) and transport mechanisms (F_{app}), can be expressed as follows:

$$\frac{\partial}{\partial t}\left(\rho_g\phi+(1-\phi)m_{ad}\right)+\nabla\cdot(-\rho_g\frac{\prod_i F_{app,i}k_0}{\mu_g}\nabla p)=\rho_g q_w \quad \text{in } \Omega_m \tag{1}$$

Similarly, the governing equation for fracture (Ω_f), only considering transport mechanisms, can be expressed as follows:

$$\frac{\partial}{\partial t}\left(\rho_g \phi\right)+\nabla\cdot(-\rho_g \frac{\prod_i F_{app,i} k_0}{\mu_g}\nabla p)=\rho_g q_w \quad \text{in } \Omega_f \tag{2}$$

Introducing inverse formation volume factor $b_g = \rho_g / \rho_{gsc}$ $(\rho_g = b_g \rho_{gsc})$, the above equation can be rewritten as follows:

$$\begin{aligned} &\frac{\partial}{\partial t}\left(b_g \phi + \frac{(1-\phi)}{\rho_{gsc}} m_{ad}\right)+\nabla\cdot(-b_g \frac{\prod_i F_{app,i} k_0}{\mu_g}\nabla p)=b_g q_w \quad \text{in } \Omega_m \\ &\frac{\partial}{\partial t}\left(b_g \phi\right)+\nabla\cdot(-b_g \frac{\prod_i F_{app,i} k_0}{\mu_g}\nabla p)=b_g q_w \quad \text{in } \Omega_f \end{aligned} \tag{3}$$

where ρ_g is the mass density of gas, M/L^3; μ_g is the dynamic viscosity of natural gas, N.T/L^2 m_{ad} is the accumulation term due to adsorption, M/L^3; ϕ is the matrix porosity, dimensionless; k_0 is the absolute Darcy permeability of the reservoir rock, L^2. $F_{app,i}$ is the i-th permeability correction factor for a specific shale gas transport mechanism; q_w is the volumetric sink/source term, M/L^3/T. k_0 is the absolute Darcy permeability of the reservoir rock, L^2.

2.1 Gas properties

Density: The pressure-dependent density of natural gas can be calculated by the real gas law:

$$\rho_g = \frac{pM}{Z(p,T)RT} \tag{4}$$

where M is the molecule weight of the natural gas, M/Mol; R is the Boltzmann constant, 8.314 ML^{2}T^{-2}/T/mole); T is the reservoir temperature, T;

The compressibility factor Z can be calculated using either implicit Peng-Robinson equation-of-state (PR-EOS) equation or empirical explicit equation. Using the empirical equation, the complex natural gas mixture can be considered as a single component with pseudo-temperature and pseudo-pressure. Mahmoud (2014) developed an explicit empirical equation for natural gas mixture as follows:

$$Z(p,T)\text{=}0.702e^{-2.5T_{pr}}\cdot p_{pr}^2 - 5.524e^{-2.5T_{pr}}\cdot p_{pr} + (0.044T_{pr}^2 - 0.164T_{pr} + 1.15) \tag{5}$$

where the reduced-temperature and reduced-pressure can be expressed as $T_{pr} = T / T_c$ and $p_{pr} = p / p_c$, respectively. T_{pc} ands P_{pc} are the pseudo-critical pressure and pseudo-critical temperature for the shale gas mixture, respectively.

Also, for single component gas simulation, such as methane, the Z factor can be accurately estimated by solving a cubic function of PR-EOS as follows (Lira and Elliott, 2012):

$$
\begin{aligned}
&Z^3 + a_2 Z^2 + a_1 Z + a_0 = 0 \\
&a_0(p,T) = (AB - B^2 - B^3),\ \ a_1(p,T) = A - 3B^2 - 2B,\ \ a_2(p,T) = B - 1 \\
&A = ap/(RT)^2,\ B = bp/(RT) \\
&a = \frac{0.457235 R^2 T_c^2}{p_c},\ \ b = \frac{0.0777961 R T_c}{p_c}
\end{aligned} \tag{6}
$$

In this paper, an analytical solution (see details in appendix B of Lira and Elliott, 2012) is used for solving the cubic equation. For more complex natural gas mixture, it requires complex flash calculation and belongs multi-component compositional simulation which will be investigated in our future work. **Fig. 3** shows an estimation of Z-factor for methane using Eq.5 and Eq. 6, respectively.

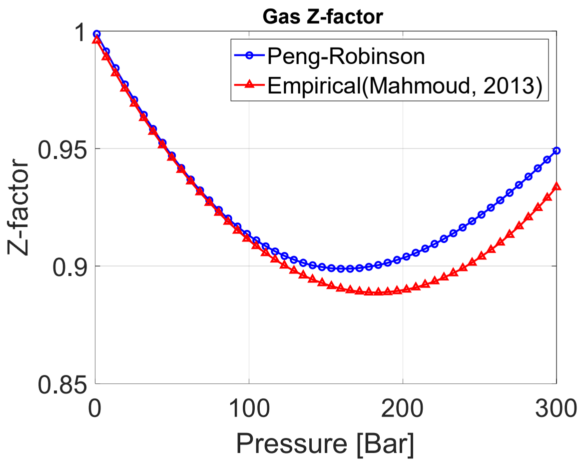

Fig. 3 Evaluated natural gas Z-factor for empirical and PR-EOS models with T=352 K, T_c=191 K, p_c=4.64 MPa, R=8.314 J/(K.mol)

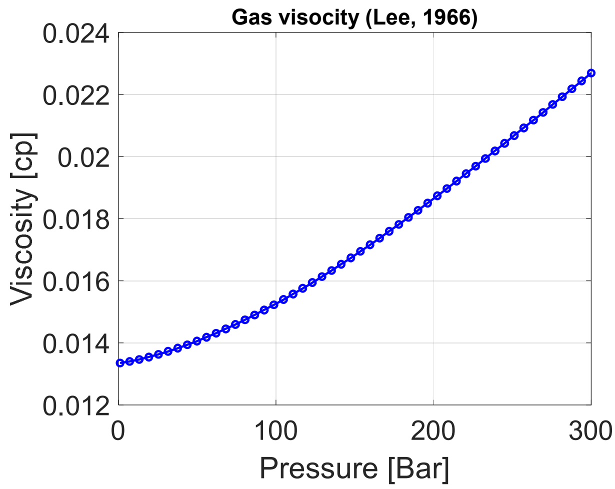

Fig. 4 Evaluated natural gas viscosity using Lee Lee-Gonzalez-Eakin empirical correlation with M=16.04 g/mol and T=633.6 Rankine

Viscosity: The density-dependent viscosity of natural gas can be estimated by Lee-Gonzalez-Eakin empirical correlation (Lee et al, 1966) as follows:

$$\mu_g = 10^{-7} K \exp(X \rho_g^Y)$$
$$K = \frac{(9.379 + 0.01607M)T^{1.5}}{209.2 + 19.26M + T}, \quad X = 3.448 + \frac{986.4}{T} + 0.01009M, \quad Y = 2.447 - 0.2224X \tag{7}$$

where the unit of M, T are g/mol and Rankine, respectively. **Fig. 4** shows an estimation of viscosity for methane using Eq.7.

Noted that although the usage of pseudo-pressure equation can eliminate the nonlinearity issue introduced by pressure-dependent gas viscosity and compressibility (Eqs. 5-6), it leads lead to even larger errors especially for tight shale reservoirs (Houze et al, 2010). Thus, in this paper, the real-gas equation is used.

2.2 Transport and storage mechanism

Since rapid commercial development of unconventional tight reservoirs in recent years, many researchers spend enormous effort to understand the transport and storage mechanism of shale gas in such complex multi-scale systems (Figs. 1-2). Several key physical mechanisms (Yu et al, 2016; Klinkenberg, 1941; Florence et al, 2007; Javadpour, 2007; Civan, 2010) can be summarized as in **Table 2**.

In the presented open-source code, *OpenShale*, any storage and transport mechanisms models can be easily implemented via defining nonlinear gas storage function (m_{ad}) and permeability correction function (F_{app}). Demonstrative storage and transport models implemented in OpenShale this study are shown as follows:

Table 2. Key transport and storage mechanism for shale gas flow

Mechanism	Models	Type	Continuum
Adsorption	Langmuir, BET	S*	Matrix
Slip flow & Diffusion	Klinkenberg, Florence, Javadpour, Civan	T*	Matrix
Non-Darcy flow	Darcy-Forchheimer	T	Fracture

*S-Storage mechanism, T-Transport mechanism

Adsorption: The gas molecules adsorbed in the pore wall of Kerogen in shale reservoir can be modeled using monolayer Langmuir isotherm and multiple layer BET isotherm as follows (Yu et al, 2016a):

$$\text{Langmuir: } m_{ad} = \rho_s \rho_{gsc} \frac{pV_L}{p+P_L} \tag{8}$$

$$\begin{gathered}\text{BET: } m_{ad} = \rho_s \rho_{gsc} \frac{V_m C p_r}{1-p_r}\left[\frac{1-(n+1)p_r^n + np_r^{n+1}}{1+(C-1)p_r - Cp_r^{n+1}}\right] \\ p_r = \frac{p}{P_s},\ P_s = \exp(7.7437 - \frac{1306.5485}{19.4362+T})\end{gathered} \tag{9}$$

where V_L is the Langmuir volume, L^3/M. P_L is the Langmuir pressure, $M/L/T^2$. ρ_s is the density of rock bulk matrix M/L^3, V_L is the Langmuir volume (the maximum adsorption capacity at a given temperature), L^3/M. P_L is the Langmuir pressure (the pressure at which the adsorbed gas volume is equal to $V_L/2$), $M/L/T^2$. V_m is the BET adsorption volume, L^3/M. C is the BET adsorption constant, dimensionless. n is the BET adsorption molecular layers, dimensionless. p_s is the pseudo-saturation pressure, $M/L/T^2$. Noted that, the unit of P_s is MPa. **Fig. 5** shows an estimation of adsorption isotherm using Eq.8 and Eq. 9, respectively.

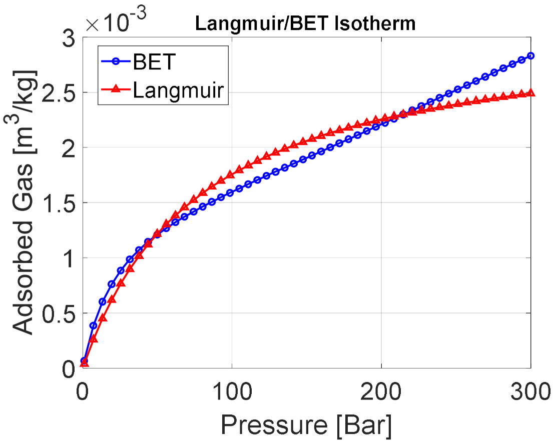

Fig. 5 Langmuir and BET isotherms curve with V_L=0.0031 m^3/kg and P_L=7.89 MPa, T=327.59 K, P_s=53.45 MPa, V_m=0.0015 m^3/kg, C=24.56 and n=4.46

Slippage flow & Diffusion: Considering slippage and diffusion effect of shale gas flow in the matrix, the apparent permeability in the low-pressure region around the fracture will be increased. In the OpenShale, the Florence's (2007) permeability correction factor (**Fig. 4**) is implemented as follows:

$$F_{app} = (1+\alpha K_n)(1+\frac{4K_n}{1+K_n}) \tag{10}$$

$$K_n = \frac{\mu_g}{2.8284 p_g}\sqrt{\frac{\pi RT}{2M}\frac{\phi}{k_0}}$$
$$\alpha = \frac{128}{15\pi^2}\tan^{-1}(4K_n^{0.4}) \tag{11}$$

where Kn is the Knudsen number, dimensionless. α is the rarefaction parameter, dimensionless. **Fig. 6** shows an estimation of gas slippage and diffusion permeability correction factor for methane using Eqs. 10-11.

Non-Darcy Flow: In case of high Forchheimer number (F_{oc}>0.11) in the hydraulic fractures, the linear Darcy flow is no longer applicable (Zeng and Grigg, 2006). The permeability correction factor (Barree and Conway, 2004) for Darcy-Forchheimer flow can be expressed as follows:

$$F_{app} = \frac{2}{1+\sqrt{1+4\rho_g \beta \left(\frac{k_0}{\mu_g}\right)^2 |\nabla p|}} \tag{12}$$

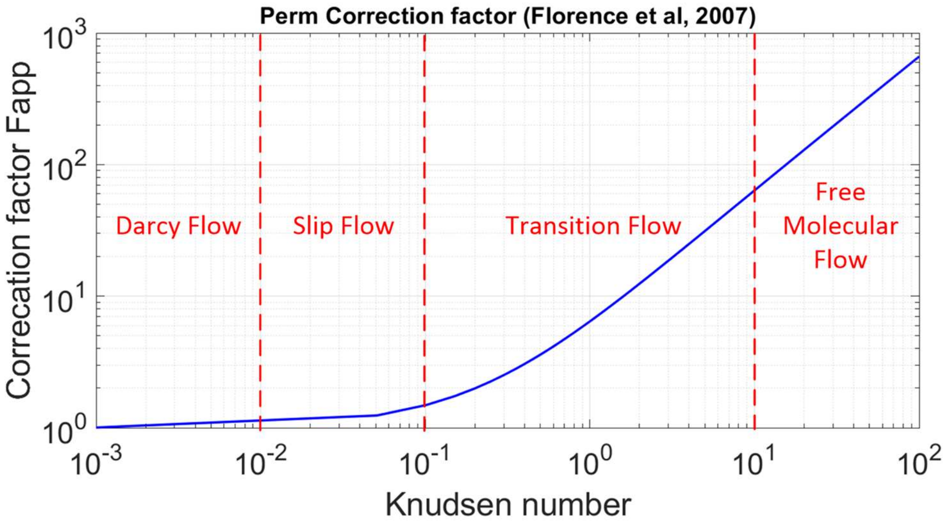

Fig. 6 – Permeability correction factor F_{app} versus Knudesen number for all flow regions with methane properties in Table 2, T=191 K, k_0=1e-10 and ϕ=0.1

where β is the empirical Forchheimer coefficient, for propped hydraulic fractures, which can be evaluated as follows (Rubin, 2010):

$$\beta = 3.2808\frac{1.485\times10^9}{(k_0\times10^{-15})^{1.021}} \tag{13}$$

2.3 Geomechanics effect

As shown in Fig. 2, shale reservoir has multi-scale fractures. The fracture conductivity will be decreased with increasing of production time due to the proppant embedment and fracture closure under high stress concentration near the fracture (Akkutlu et al, 2018, Hu et al, 2018a, 2018b). In this paper, three types of fractures are defined based on their various length scales, including hydraulic fracture (half-length 50-100 meters, aperture 1mm), natural fracture (half-length 1-20 m, aperture 0.1mm), and micro-fracture (half-length < 1m, aperture <0.1 mm). A new geomechanics model is proposed herein by considering closure of micro-fracture, unpropped natural fracture and propped fractures.

To consider the micro-fracture closure, Gangi's (1978) empirical pressure-dependent permeability reduction model can be applied as follows:

$$k = k_0 F_{app} = k_0 \left[1 - \left(\frac{P_c - \alpha_B p}{P_1} \right)^m \right]^3 \tag{14}$$

Where α_B is the Biot's constant, P_c is the confining overburden pressure, P_1 is the effective stress when micro-fracture completely closed. m is a constant related to surface roughness. **Fig. 7** shows an estimation of Gangi permeability correction factor for methane using Eqs. 14.

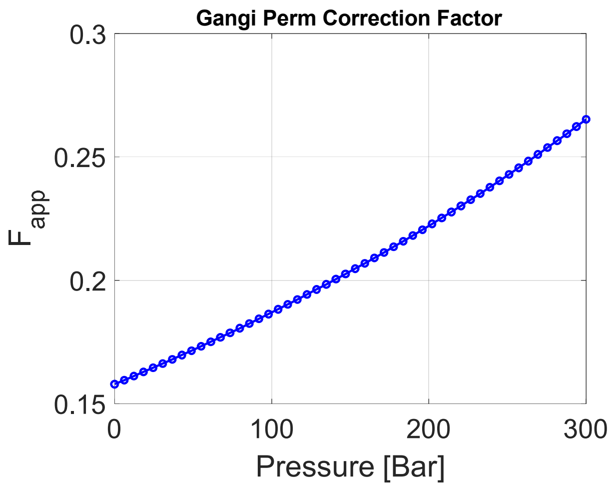

Fig. 7 – Permeability correction factor F_{frac} versus pore pressure with m=0.5, p_1=180 MPa, p_c=38 MPa and α=0.5

To consider the closure of hydraulic and natural fractures, Alramahi and Sundberg (2012) performed experiment to measure the effect of closure pressure on propped fracture conductivity for different shale samples from stiff shale to soft shale. An empirical model of normalized fracture conductivity for propped fractures, $F_{cd,N}$, can be fitted as follows:

$$\begin{aligned} &\text{Stiff Shale: } \mathrm{F}_{cd,N}(p) = 10^{-0.00011\sigma - 0.0971}, \quad \mathrm{R}^2 = 0.961 \\ &\text{Meidum Shale: } \mathrm{F}_{cd,N}(p) = 10^{-0.00035\sigma + 0.2396}, \quad \mathrm{R}^2 = 0.996 \\ &\text{Soft Shale: } \mathrm{F}_{cd,N}(p) = 10^{-0.00064\sigma - 0.4585}, \quad \mathrm{R}^2 = 0.987 \end{aligned} \tag{15}$$

 doi:10.20944/preprints202001.0080.v1

Wu et al (2018) performed similar experiment to investigate the effect of closure pressure on unpropped fracture conductivity. An empirical model of normalized fracture conductivity for unpropped fractures can be fitted as follows:

$$\begin{aligned}
&\text{Stiff Shale: } \mathrm{F}_{cd,N}(p)=10^{-0.793\ln(\sigma_c)+4.5618},\quad \mathrm{R}^2=0.995\\
&\text{Meidum Shale: } \mathrm{F}_{cd,N}(p)=10^{-0.89\ln(\sigma_c)+5.0725},\quad \mathrm{R}^2=0.988\\
&\text{Soft Shale: } \mathrm{F}_{cd,N}(p)=10^{-1.041\ln(\sigma_c)+6.0216},\quad \mathrm{R}^2=0.989
\end{aligned} \tag{16}$$

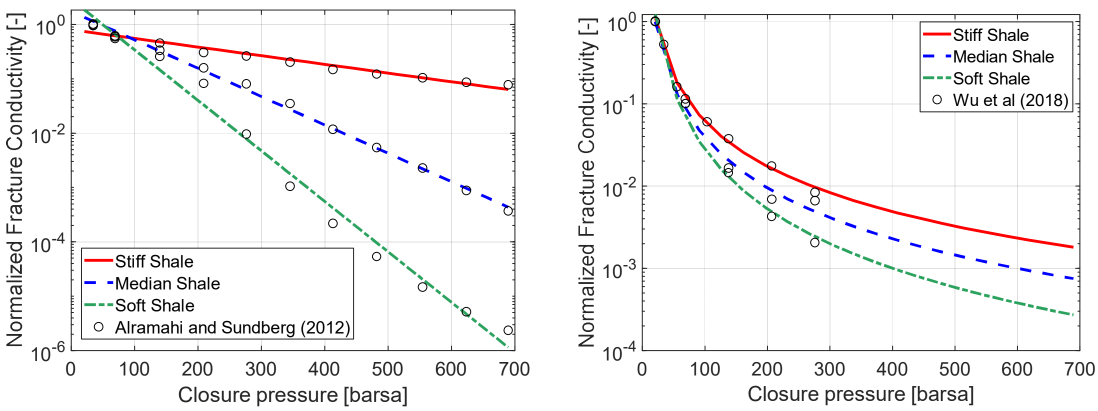

(a) (b)

Fig. 8 – Empirical correlation between normalized fracture conductivity and closure pressure for propped fractures (a) and unpropped fractures (b)

Where effective closure stress σ_c can be calculated by reservoir horizontal stress and in-situ fracture pore pressure, $\sigma_c(p)=\sigma_h-p$. Plane direction of hydraulic fracture is normally orthogonal to the minimum horizontal stress and it support by rigid proppant, while the plane of natural fracture has stochastic orientation and lacking support from proppant. Thus, the closure stress for hydraulic fracture and natural fracture can be expressed as follows:

$$\begin{aligned}
&\text{HydraulicFrac: } \sigma_{HF}=\sigma_{h\min}-p\\
&\text{NaturalFrac: } \sigma_{NF}=\frac{\sigma_{h\min}+\sigma_{h\max}}{2}-p
\end{aligned} \tag{17}$$

The empirical correlation between fracture conductivity and closure pressure are shown in **Fig. 8**. In the OpenShale, the fracture permeability can be reduced by a dynamic permeability correction factor as follows:

$$k_f=k_0F_{app}=k_0\frac{F_{cd}(p)}{F_{cd}(p_0)} \tag{18}$$

Based on proposed empirical correlation model in Eqs. 15-16, a typical permeability correction factors for fracture closure can be shown as follows (**Fig. 9**):

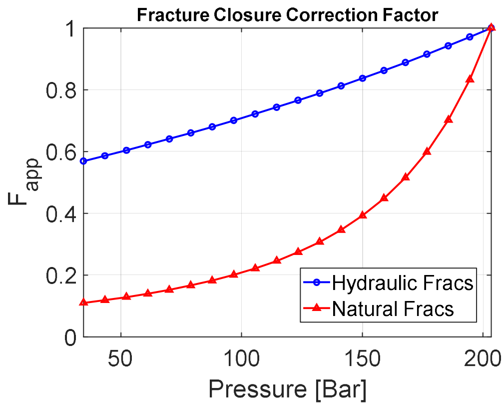

Fig 9 – Permeability correction factor F_{frac} for hydraulic fractures and natural fractures with p_o = 20.34 MPa and p_{wf} = 34.5 MPa $\sigma_{h\min}$ = 29 MPa and $\sigma_{h\max}$ = 34 MPa

3 Numerical Model

In this paper, a new shale gas simulation framework, OpenShale , is developed using the automatic differentiation module (ad-core, ad-props), black-oil module (ad-blackoil) and hierarchical fracture model (hfm) module in open-source MATLAB Reservoir Simulation Toolbox (Lie, 2012). Two-point flux approximated finite volume method (TPFA-FVM) is applied for discretizing the governing equations (Eq. 3). Time discretization is implemented using a fully implicit first-order backward scheme, where the Jacobian matrix of the nonlinear system is calculated by Automatic Differentiation. All nonlinear functions for shale gas transport and storage mechanisms as well as geomechanics effect are defined as separate function. For multi-scale fracture system, the larger fracture, such as the hydraulic fracture and natural fracture are explicitly modeled using EDFM. The micro-fractures are assumed highly connected and thus upscaled into the matrix permeability.

3.1 Numerical discretization

The discretized governing equation of Eq. 3 can be expressed as follows:

$$\begin{aligned}&\frac{\phi V}{\Delta t}\left(b_g(p^{n+1})-b_g(p^n)\right)+\frac{(1-\phi)V}{\Delta t}\frac{1}{\rho_{gsc}}\left(m_{ad}(p^{n+1})-m_{ad}(p^n)\right)\\&-\mathbf{div}\left(b_g(p^{n+1})\frac{\prod_i F_{app,i}(p^{n+1})}{\mu_g(p^{n+1})}T\cdot\mathbf{grad}(p^{n+1})\right)\\&-Vb_g(p^{n+1})q_w(p^{n+1})-Vb_g(p^{n+1})\psi_{f-m}(p^{n+1})=0\end{aligned}\tag{19}$$

The discretized governing equation for each 1D fracture system can be expressed as follows:

$$\begin{aligned}&\frac{\phi V}{\Delta t}\left(b_g(p^{n+1})-b_g(p^n)\right)\\&-\mathbf{div}\left(b_g(p^{n+1})\frac{\prod_i F_{app,i}(p^{n+1})}{\mu_g(p^{n+1})}T\cdot\mathbf{grad}(p^{n+1})\right)\\&-Vb_g(p^{n+1})q_w(p^{n+1})-Vb_g(p^{n+1})\psi_{m-f}(p^{n+1})=0\end{aligned}\tag{20}$$

where V is the bulk volume of a grid cell. $\psi_{f-m/m-f}$ is the flow coupling term between fracture and matrix. To simplify the implementation of governing equations (Eqs. 18-19), three discrete domain delta δ functions for matrix (Ω_m), hydraulic fractures (Ω_{HF}) and natural fractures (Ω_{NF}) can be defined as follows:

$$\delta_m(x)=\begin{cases}1 & x\in\Omega_m\\0 & x\notin\Omega_m\end{cases},\quad \delta_{HF}(x)=\begin{cases}1 & x\in\Omega_{HF}\\0 & x\notin\Omega_{HF}\end{cases},\quad \delta_{NF}(x)=\begin{cases}1 & x\in\Omega_{NF}\\0 & x\notin\Omega_{NF}\end{cases}\tag{21}$$

A generic numerical model for fractured reservoir considering shale gas transport and storage mechanism can be expressed as follows:

$$\begin{aligned}&\frac{\phi V_{ijk}}{\Delta t}\left(b_g(p^{n+1})-b_g(p^n)\right)+\delta_m\frac{(1-\phi)V_{ijk}}{\Delta t}\frac{1}{\rho_{gsc}}\left(m_{ad}(p^{n+1})-m_{ad}(p^n)\right)\\&-\mathbf{div}\left(b_g(p^{n+1})\frac{\prod_i\left[1+\delta_{HF/NF,i}F_{app,i}(p^{n+1})\right]}{\mu_g(p^{n+1})}T\cdot\mathbf{grad}(p^{n+1})\right)\\&-V_{ijk}b_g(p^{n+1})q_w(p^{n+1})-V_{ijk}b_g(p^{n+1})\psi_{f-m/m-f}(p^{n+1})=0\end{aligned}\tag{22}$$

Assuming vertical well fully penetrate the reservoir thickness, a semi-analytical well model (Peaceman, 1983) for a vertical well can be expressed as follows:

$$q_w=WI/\mu_g(p_{bh}-p)\tag{23}$$

where p_{bh} is the bottom hole pressure of a wellbore, M/L/T^2. WI is the wellbore flow index.

The solution matrix from Eqs. 21 can be expressed as follows:

$$\begin{bmatrix}\mathbf{A}_{mm} & \mathbf{A}_{mf} & \mathbf{A}_{mw}\\ \mathbf{A}_{fm} & \mathbf{A}_{ff} & \mathbf{A}_{fw}\\ \mathbf{A}_{wm} & \mathbf{A}_{wf} & \mathbf{A}_{ww}\end{bmatrix}\begin{Bmatrix}\mathbf{p}_m\\ \mathbf{p}_f\\ \mathbf{p}_w\end{Bmatrix}=\begin{Bmatrix}\mathbf{Q}_m\\ \mathbf{Q}_f\\ \mathbf{Q}_w\end{Bmatrix}\tag{24}$$

$$\#\mathbf{p}_m=\#\text{MatrixEles},\quad \#\mathbf{p}_f=\#\text{FractureEles},\quad \#\mathbf{p}_w=\#\text{Eles has well}$$

Noted that the shale gas viscosity, density and permeability corrections terms are all depends on solution variables. To solve non-linear system of Eq. 23, the residual form of Newton's iterations can be expressed as follows:

$$\mathbf{J}(\mathbf{x}^i)(\mathbf{x}^{i+1}-\mathbf{x}^i)=\frac{d\mathbf{R}}{d\mathbf{x}}(\mathbf{x}^i)(\mathbf{x}^{i+1}-\mathbf{x}^i)=-\mathbf{R}(\mathbf{x}^i) \tag{25}$$

The Jacobian matrix **J** is calculated by automatic differentiation in MRST.

3.2 EDFM

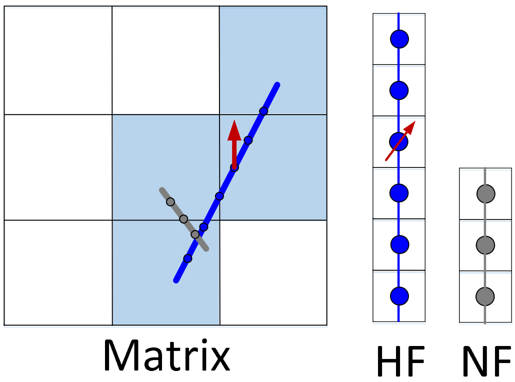

Fig. 10 – Grid system in EDFM for matrix, natural fracture and hydraulic fracture

As shown in **Fig. 10**, EDFM adopted the concept of dual-continuum fracture modeling method, the flow coupling term $\psi_{f-m/m-f}$ is introduced to couple the solution among matrix and fractures. Thus, the matrix grid is not necessary conforming with the fracture plane. As shown in **Fig. 11**, there are three kinds of non-neighbor connection (NNC) in EDFM formulation: 1) fracture-matrix connectivity, 2) fracture-fracture connectivity and 3) fracture-well connectivity. The general NNC model can be expressed as follows (Xu, 2015):

$$\begin{aligned}\psi_{f-m}^{NNC}&=T_{f-m}^{NNC}(p_f^{n+1}-p_m^{n+1})\\ \psi_{f-m}^{NNC}&=-\psi_{m-f}^{NNC}\end{aligned} \tag{26}$$

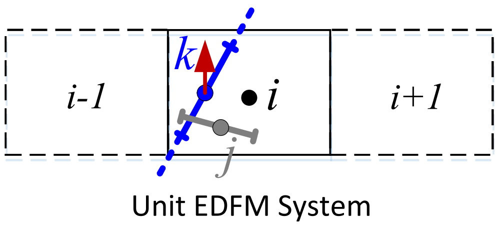

Fig. 11 – Unit EDFM NNCs of 1) fracture-matrix (*i-k* pair) connectivity 2) fracture-fracture (*j-k* pair) connectivity and 3) fracture-wellbore (well-*k* pair) connectivity

Fracture-matrix NNC: The fracture-matrix transmissibility (T_{f-m}) can be expressed as follows:

$$T_{ik}^{NNC} = \frac{k_{0,ik}}{\mu_{g,ik}} \frac{A_{ik}}{\langle d \rangle_{ik}} \tag{27}$$

where $A_{i,k}$ is the intersection area fraction between a fracture plane and a gridblock. For 2D grid, the area is the product of intersected fracture cell length within the matrix cell and uniform formation thickness, *DZ*. Noted that the harmonic average and upwind scheme are used for the permeability and viscosity, respectively. $\langle d \rangle_{i,k}$ is the average normal distance between matrix cell and fracture plane, which can be calculated as follows:

$$\langle d \rangle_{ik} = \frac{\int d_{ik} dv}{V_i} \tag{28}$$

For 2D structured grid, an analytical solution is available for the average normal distance (see Tene et al, 2016).

Fracture-fracture NNC: the star-delta transformation can be used to calculate the transmissibility between intersected fractures as follows (Hajibeygi et al, 2011):

$$T_{jk}^{NNC} = \frac{t_j t_k}{\sum_{m=1}^{N_{ints}} t_m}, \quad t_m = \frac{A_{f,m}}{0.5 h_{f,m}} \frac{k_{0,m}}{\mu_{g,m}} \tag{29}$$

where A_f is the cross-section area of a fracture plane, for 2D cell, which can be calculated by product of fracture aperture, w_f, and formation thickness. h_f is the fracture cell length.

Fracture-well NNC: If a well intersected with a fracture cell, the effective wellbore index (WI) and equivalent radius (r_e) can be expressed as follows (Xu, 2015):

$$WI_f = \frac{2\pi k_f w_f}{\ln(r_e / r_w) + s}, \quad r_e = 0.14\sqrt{h_f^2 + DZ^2} \tag{30}$$

where s is the skin factor, dimensionless, which will be used as a correction factor to correct the error introduced by EDFM when model low-permeability fractures. *DZ* is the formation thickness, L.

4 Verification

To verify the presented general shale gas model (Eq. 21), two numerical simulations are performed against a commercial simulator (CMG, 2015) and an in-house simulator with unstructured mesh (Jiang and Younis, 2015). The base model and simulation parameters for all cases as shown in **Table 3**:

Table 3—Base model and simulation parameters for all cases

Property	Unit	Value

Rock density	kg/m^3	2500
Molecular weight, CH_4	kg/mol	0.01604
Critical pressure, CH_4	MPa	4.60
Critical temperature, CH_4	K	190.6
Acentric factor, CH_4	-	0.01142
Well radius	m	0.1

4.1 Case 1 – Verification against commercial simulator

OpenShale is firstly verified in a simple methane production case against a commercial simulator (CMG) with a single vertical hydraulic fracture (**Fig. 12**). By changing the hydraulic conductivity, grid schemes and natural fractures, three subcases (Case1a, Case1b and Case1c) are investigated. The accuracy of OpenShale with explicit fracture modeling (EFM) and EDFM are systematically studied. In this simulation, only Langmuir adsorption (Eq. 8) is considered. All fluid properties and simulation parameters are the same with the commercial simulator. The compressibility factor Z and natural gas viscosity are directly interpolated from the properties table of the commercial simulator. Detailed simulation properties are shown in **Table 4.**

Table 4. Key reservoir and simulation parameters of Case 1

Property	Unit	Value
Domain dimensions (x,y)	m	606.6,606.6
Grid (nx,ny)	-	201,65
Formation thickness	m	45.72
Initial reservoir pressure	MPa	34.47
Temperature	K	327.60
Langmuir pressure	MPa	8.96
Langmuir volume	m^3/kg	0.0041
Matrix porosity		0.07
Matrix compressibility	1/Pa	1.45e-10
Matrix permeability	nD	500
Fracture permeability	mD	0.5-1000
Fracture width	m	0.003
Fracture half-length	m	106.68
Fracture conductivity	md-ft	5-10000
Well BHP	MPa	3.45
Production time	years	30

Preprints (www.preprints.org) | NOT PEER-REVIEWED | Posted: 9 January 2020 doi:10.20944/preprints202001.0080.v1

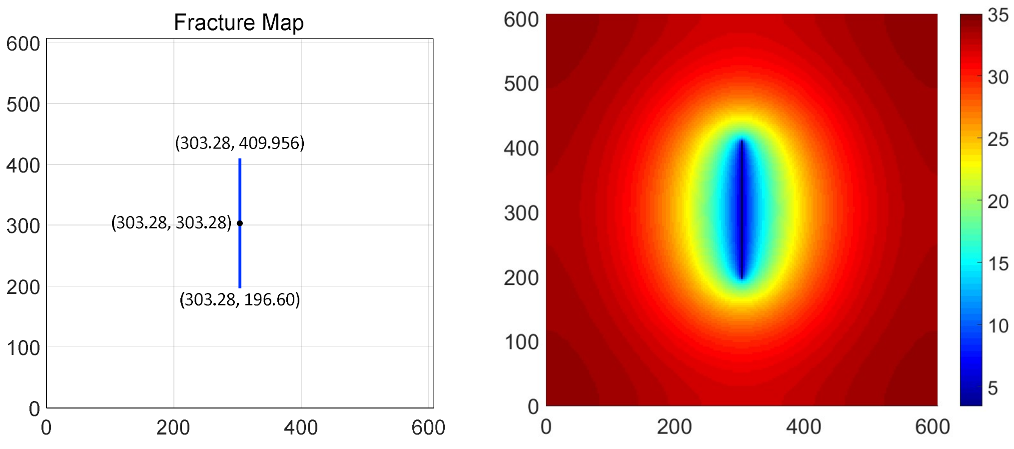

(a) (b)

Fig. 12 Fracture map (a) and pressure contour after 30 years production (b) of Case 1a and Case1b

Case1a: In the first subcase, three fracture conductivities (10000 md-ft, 50 md-ft, 5 md-ft) are used to verify the accuracy of OpenShale with EFM and EDFM. **Fig. 13** shows a good agreement of both gas flow rate and cumulative production between OpenShale and commercial simulator. Results show that OpenShale with EFM (dash line) always gives consistent results against commercial simulator. But OpenShale with EDFM (solid) has significant error (up to 10.92%) when fracture conductivity is low (5 md-ft). Fig. 12a shows that OpenShale EDFM only converges to reference solution under infinite fracture conductivity (10000 md-ft). This is observation matches Tene (2017)'s conclusion that EDFM can not handle the fracture with low permeability.

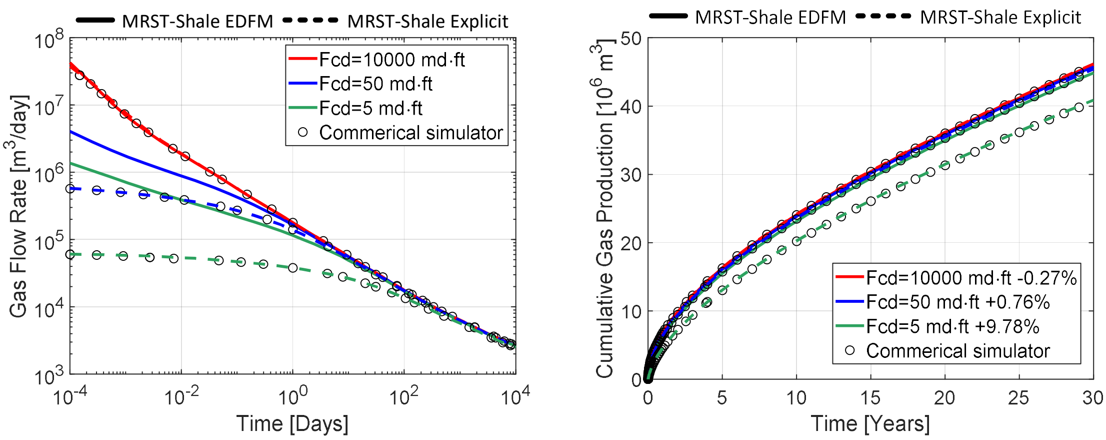

(a) log-log gas flow rate (b) cumulative production

Fig. 13 Comparison of gas flow rate (a) and cumulative production (b) for Case 1a between OpenShale EDFM (solid line), OpenShale EFM (dash line) and a commercial

Preprints (www.preprints.org) | NOT PEER-REVIEWED | Posted: 9 January 2020 doi:10.20944/preprints202001.0080.v1

simulator (dots) with respect to fracture conductivities of 5 md-ft (green lines), 50 md-ft (blue lines) and 10000 md-ft (red lines)

Case1b: For unconventional tight reservoir, LGR is usually required to capture the transient flow behavior and sharp pressure gradient near the hydraulic fractures. In the second subcase, the effect of grid schemes on accuracy of OpenShale with EFM and EDFM are investigated. In this case, the fracture conductivity is set as 10000 md-ft to eliminate the EDFM error mentioned in Case1a. All other parameter is the same with Case1a. As shown in **Fig. 14**, three grid schemes are investigated, where LGR scheme with logarithmic refinement that is solved by OpenShale EFM; EDFM scheme is the standard EDFM grid scheme (Xu et al, 2017 and Tene et al, 2017) with uniform grid that is solved by EDFM; EDFM+LGR scheme is the same grid scheme as LGR scheme that an additional EDFM fracture cell is added and that is solved by EDFM. Noted that all grid scheme has the same grid dimension (nx,ny) of 499x61.

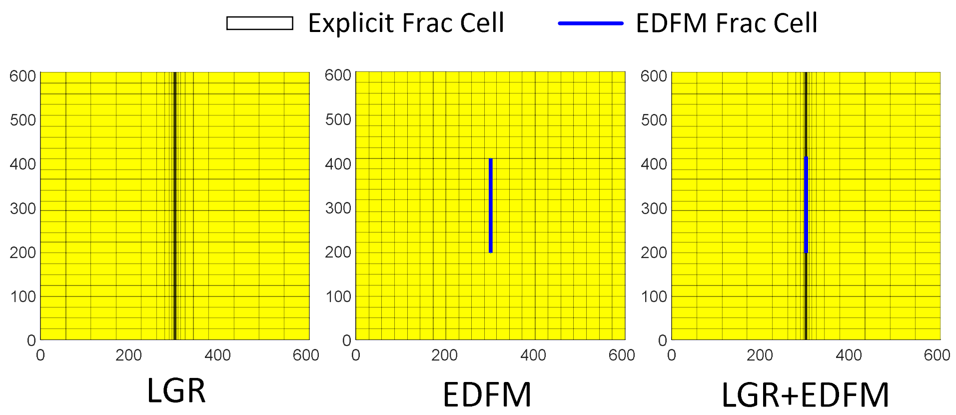

Fig. 14 EFM and EDFM Grid schemes for Case1b, fracture cell is shown 10 times larger than the real size, where logarithmic refinement and uniform used in LGR and EDFM scheme, respectively

Figs. 15-16 shows a good agreement of gas flow rate and cumulative production between OpenShale and commercial simulator with respect to high fracture conductivity and low fracture conductivity. OpenShale with EFM again gives consistent results against commercial simulator for all grid schemes. However, the standard EDFM grid scheme can introduce an error of 3.31% for high fracture conductivity and 1.11% for low fracture conductivity. The error is measured by the difference of cumulative production between grid schemes of LGR+EDFM and EDFM. This

 doi:10.20944/preprints202001.0080.v1

benchmark case demonstrates that EDFM cannot capture transient flow behavior and sharp pressure gradient near the hydraulic fracture without helping of LGR.

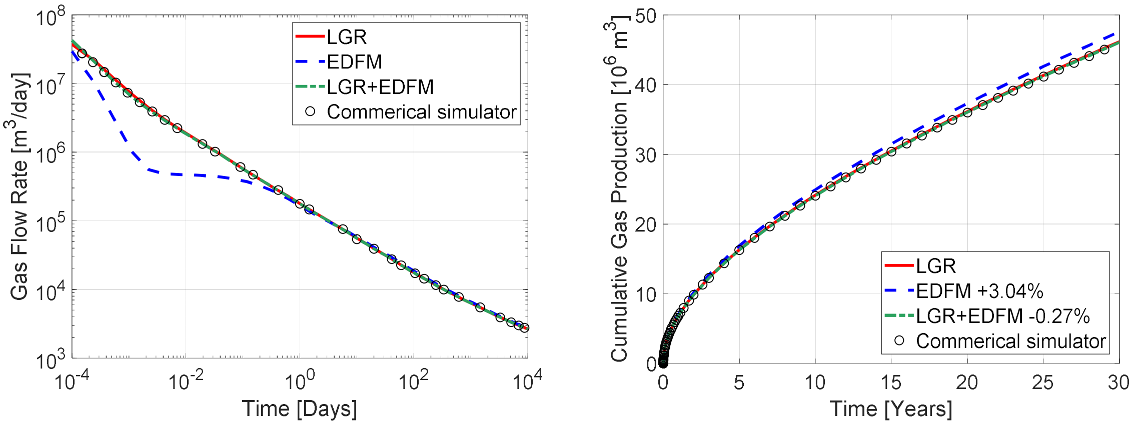

(a) log-log gas flow rate (b) cumulative production

Fig. 15 Comparison of gas flow rate (a) and cumulative production (b) for Case 1b with high fracture conductivity of 10000 md-ft between OpenShale and a commercial simulator (dots)

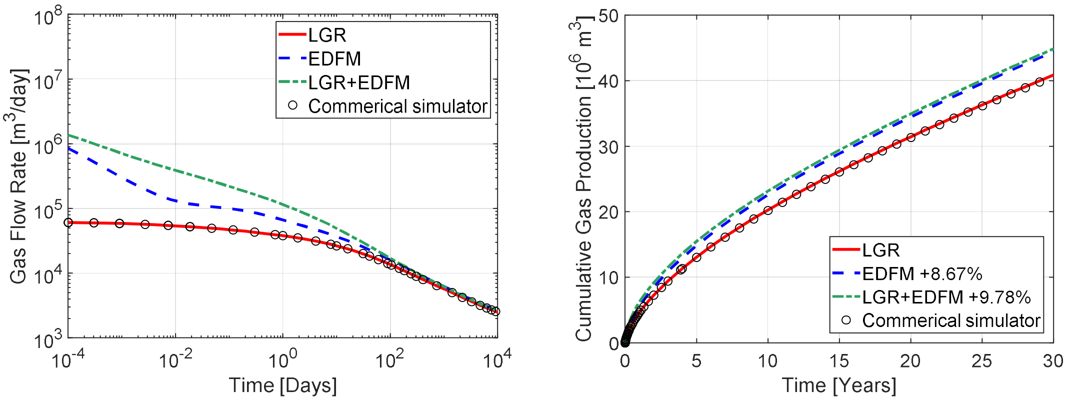

(a) log-log gas flow rate (b) cumulative production

Fig. 16 Comparison of gas flow rate (a) and cumulative production (b) for Case 1b with low fracture conductivity of 5 md-ft between OpenShale and a commercial simulator (dots)

Case1c: As mentioned in Case1a and Case1b, EDFM cannot handle low-permeability fracture and hydraulic fractures with sharp pressure gradient. But modeling of natural fracture network is quite challenge for the EFM. In this subcase, the effect of different grid schemes of natural fractures on accuracy for OpenShale with EDFM is also investigated. As shown in **Fig. 17**, six natural fractures with the same length of 116.74 m are added based on the Case1a. The well performance of two grid schemes with and without LGR for natural fractures are studied. Fracture conductivity for

Preprints (www.preprints.org) | NOT PEER-REVIEWED | Posted: 9 January 2020 doi:10.20944/preprints202001.0080.v1

hydraulic fracture and natural fractures are set as 10000 md-ft and 5 md-ft, respectively. All other parameters are the same with Table 3.

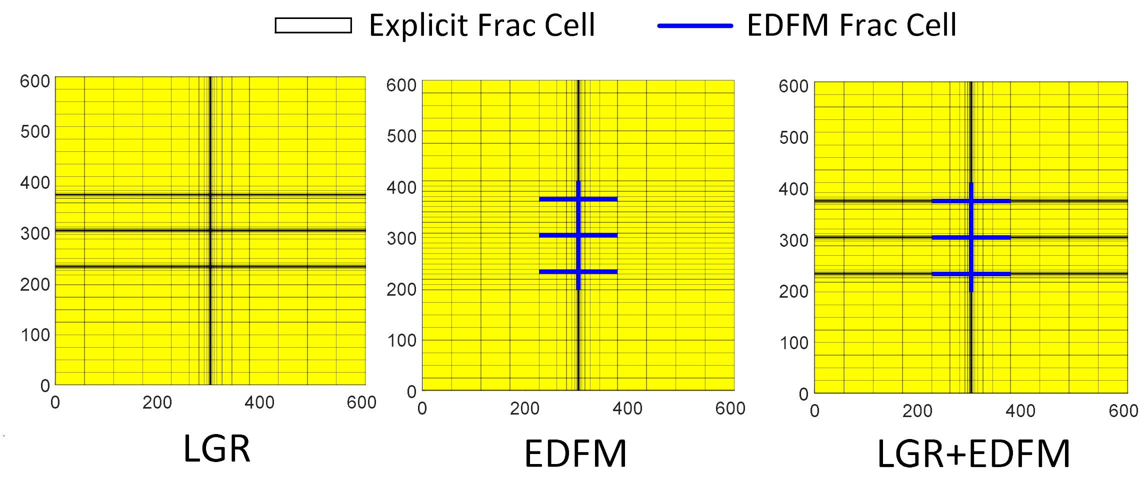

Fig. 17 Grid schemes of Case 1c, number of grids are shown 20 times coarser than the real scheme. LGR scheme with LGR for natural fractures, EDFM scheme without LGR for natural fractures

Fig. 18 demonstrates that OpenShale with EDFM can lead to a significant error (up to 16.99%) for the case where low-permeability natural fractures connected with high-permeability hydraulic fractures. Also, EDFM without LGR for natural fractures tends to underestimate the well performance (error of 3.4% for six natural fractures). This benchmark case indicates that EDFM is not capable to accurately model well performance of shale gas flow in ultra-tight reservoir due to the errors introduced by low-permeability fracture and grid refinement.

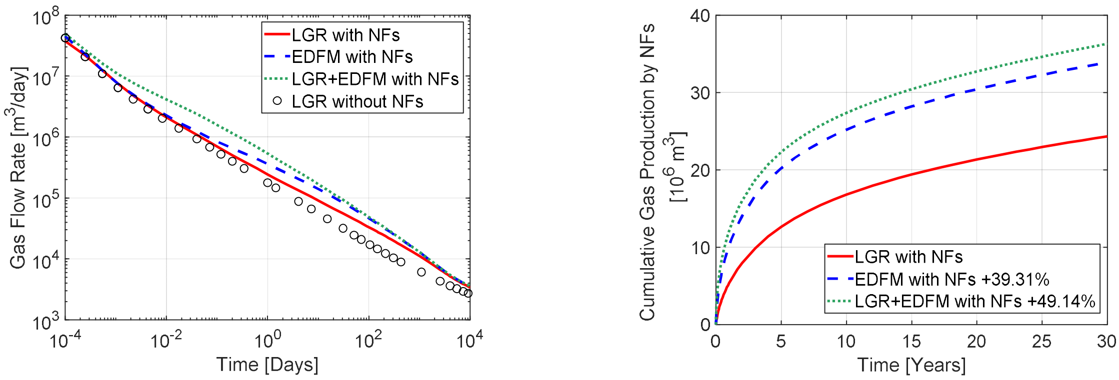

(a) log-log gas flow rate (b) normalized cumulative production

Fig. 18 Comparison of gas flow rate (a) and normalized cumulative production by NFs (b) for Case 1c between different grid scheme for natural fractures

In sum, this case study shows that OpenShale with EFM always give consistence results against commercial simulator, while OpenShale with EDFM only converge to the reference solution at infinite fracture conductivity (Case1a). Also, OpenShale with EDFM cannot handle low-permeability fracture (Case1b) and cannot capture transient behavior and sharp gradient without LGR (Case1c). OpenShale with EDFM can model complex and irregular natural fractures accurately and efficiently. Thus, in the following simulations, an empirical skin-factor and uniform grid refinement are adopted to relieve the limitations of EDFM. More advanced projected EDFM (Tene et al, 2017) and adaptively grid refinement will be implemented in our future work.

4.2 Case 2 – Verification against in-house simulator

OpenShale is further verified against an in-house simulator (Jiang and Younis, 2015) by considering more comprehensive state-of-art transport mechanisms and fracture geometries. For the reference solution, it used fully unstructured mesh with LGR to capture the complex fracture geometries as well as the sharp pressure gradient near the fracture. In this case, the gas rate solution of two sub-case are investigated. In the first sub-case (Case2a), the well performance with and without storage (Eq. 8) and transport mechanism (Eq. 10) is considered. In the second sub-case (Case2b), the irregular fracture geometry is considered. The fracture map of Case2a is shown in **Fig. 19**. Detailed simulation parameters for Case 2 are elaborated in **Table 4**.

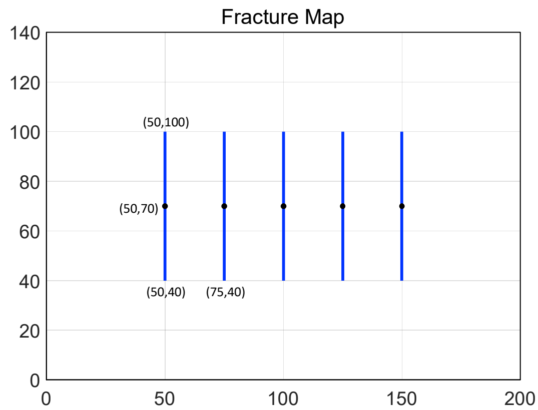

Fig. 19 Fracture map and EDFM grid of Case 2

Table 4. Key reservoir and simulation parameters of Case 2

Property	Unit	Value
Domain dimensions (x,y)	m	200,140
Formation thickness,	m	10
Initial reservoir pressure	MPa	16
Temperature	K	343.15
Langmuir pressure	MPa	4

Preprints (www.preprints.org) | NOT PEER-REVIEWED | Posted: 9 January 2020 doi:10.20944/preprints202001.0080.v1

Langmuir volume	m^3/kg	0.018
Matrix porosity		0.1
Matrix compressibility	1/Pa	1.0e-9
Fracture porosity		1.0
Matrix permeability	nD	100
Fracture permeability	D	1
Fracture width	m	1e-3
Well BHP	MPa	4
Correction skin factor	-	43
Production time	days	10000

Other parameters are the same as in Table 2

Fig. 20 shows pressure contour after 2500 days of production for Case 2 with and without transport mechanisms. It can be observed that the sub-case with full mechanism has better pressure depletion (dark blue region) than one without any mechanism. **Fig. 21** shows a good agreement between gas flow rate between OpenShale and an in-house simulator, where demonstrates that the both adsorption and gas slippage and diffusion effect increase the gas production significantly. In tight unconventional reservoirs, smaller pore-throat and lower bottom-hole pressure can lead to higher production due to gas slippage flow and releasing adsorbed gas.

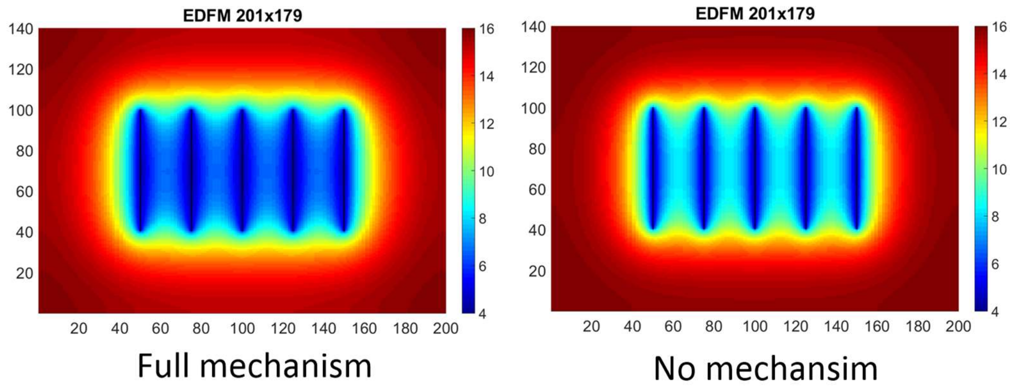

Fig. 20 Pressure contour with and without full shale gas transport mechanism @ 2500 days of Case 2

Preprints (www.preprints.org) | NOT PEER-REVIEWED | Posted: 9 January 2020 doi:10.20944/preprints202001.0080.v1

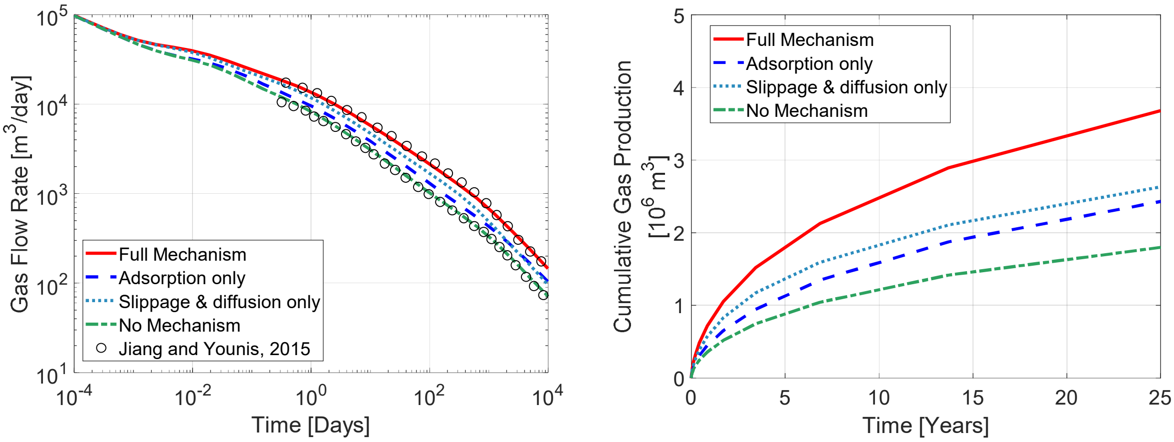

(a) log-log gas flow rate (b) cumulative production

Fig. 21 Comparison of gas flow rate (a) and cumulative production (b) for Case 2a between OpenShale and an in-house simulator

5 Application

In the previous sections, OpenShale shows it capability to handle arbitrary transport and storage mechanism and fracture geometries. To further illustrate the applicability of OpenShale in practical problems, two case studies of OpenShale in realistic unconventional reservoirs with complex fracture network are presented.

5.1 Case 3: History matching and production forecast

To further verify the applicability of the OpenShale. A history matching with field production data on a Barnett shale has performed. The field production and simulation data are adopted from literature (Cao, Liu and Leong, 2016; Yu and Kamy Sepehrnoori, 2014). The detailed reservoir and fluid parameters are shown as in **Fig. 22** and **Table 5**.

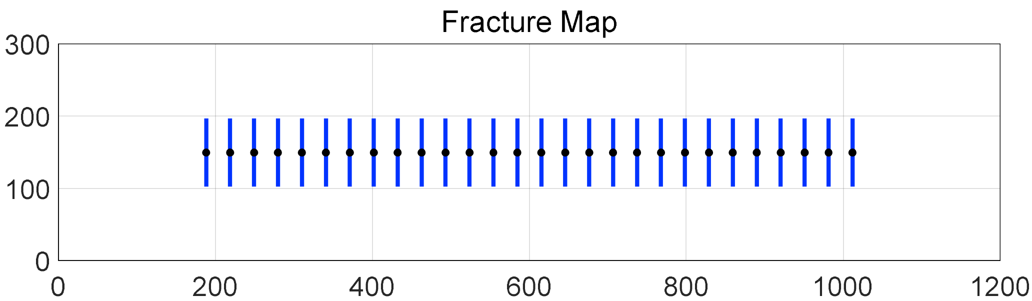

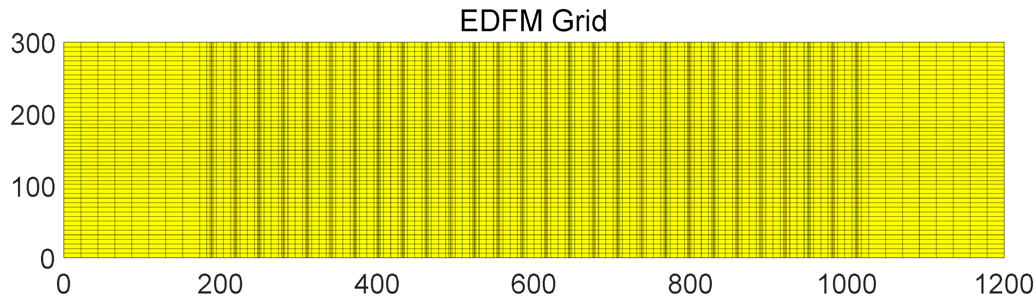

Fig. 22 Fracture map and EDFM LGR grid with 28 planar hydraulic fractures of Case 3

Table 5. Key reservoir and simulation parameters of Barnett shale for Case 3 (Cao, 2016)

Property	Unit	Value
Domain dimensions (x,y)	m	1200,300
Depth	m	5463
Formation thickness,	m	90
Initial reservoir pressure	MPa	20.34
Temperature	K	352
Rock density	kg/m^3	2500
Langmuir pressure	MPa	4.47
Langmuir volume	m^3/kg	0.00272
Matrix porosity		0.03
Matrix compressibility	1/Pa	1.5e-10
Fracture compressibility	1/Pa	1.0e-8
Matrix permeability	nD	200
Fracture permeability	mD	100
Fracture width	m	0.003
Fracture spacing	m	30.5
Fracture half-length	m	47.2
Fracture conductivity	md-ft	1
Well BHP	MPa	3.69
Correction skin factor	-	19
Production time	days	1600

Other parameters are the same as in Table 2

In this simulation, a rectangle reservoir with dimension of 1100 × 290 × 90 m was discretized by 148 × 39 × 1 grids. 28 stages hydraulic fractures in the center of domain with the half-length of 47.2 m and the fracture spacing of 30.5 m. The fractures are assumed have constant aperture of 0.003 m and permeability of 100 md. Only shale gas storage mechanism of Langmuir adsorption (Eq. 8) is considered. **Fig. 23** shows the pressure contour at different production time (400 days and 1600 days). **Fig. 24** shows the comparison of production rate between OpenShale and field data which shows good agreements with the field production data. Based on matched simulation parameters, the production forecast can be easily performed as in Fig. 21.

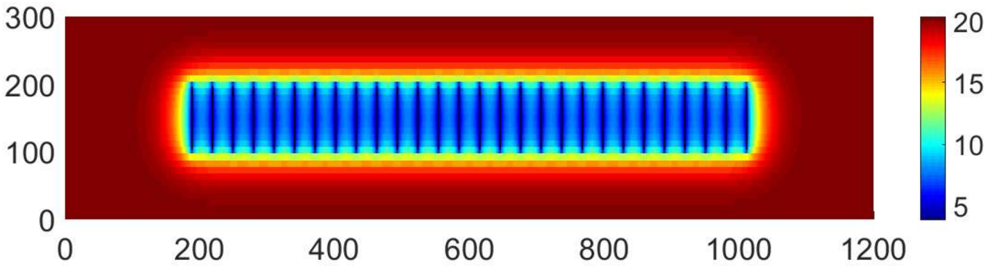

Figure 23 Pressure contour after 1600 days production for Barnett shale reservoir (Case 3)

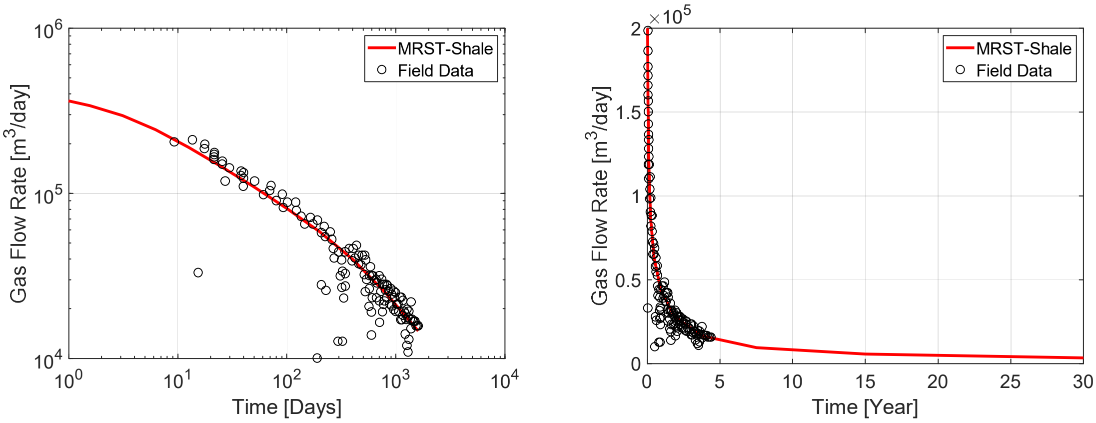

(a) (b)

Fig. 24 History matching (a) and production forecast (b) of a Barnett shale well (Case 3)

5.2 Case 4: New model evaluation

To illustrate the capability of modular design and rapid prototyping of OpenShale, a new shale gas model considering geomechanics effect (Eqs. 15-17) for multi-scale fractured network is implemented and evaluated using OpenShale. In this section, the influence of multi-scale fracture network and geomechanics effect on shale gas production performance will be investigated.

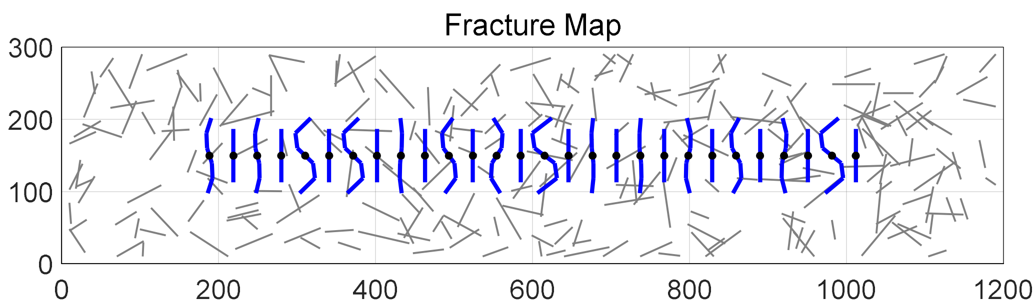

Fig. 25 Fracture map with 28 non-planar hydraulic fractures and 248 natural fractures of Case 4

In this case, all the simulation parameters are the same with Case 3 of Barnett shale reservoir. The total length of non-planar hydraulic fractures (blue lines in **Fig. 25**) is the same as planar fractures used in Case 3 (blue lines in Fig. 14). Natural fractures are stochastically generated by an open-source fracture generator ADFNE (Alghalandis, 2017). The geomechanics parameters for shale reservoir are assumed (Wasaki and Akkutlu, 2015) as follows (**Table 5**):

Table 5. Geomechanics parameters of Barnet shale for Case 4

Property	Unit	Value
Biot constant, α	-	0.5
Overburden confining stress, p_c	MPa	38
Maximum horizontal stress, s_{hmax}	MPa	34
Minimum horizontal stress, s_{hmin}	MPa	29
Maximum closure stress for micro-fracture, p_l	MPa	180
Gangi exponential constant, m	-	0.5
Natural fractures permeability	md	10

Other parameters are the same as in Tables 2-3

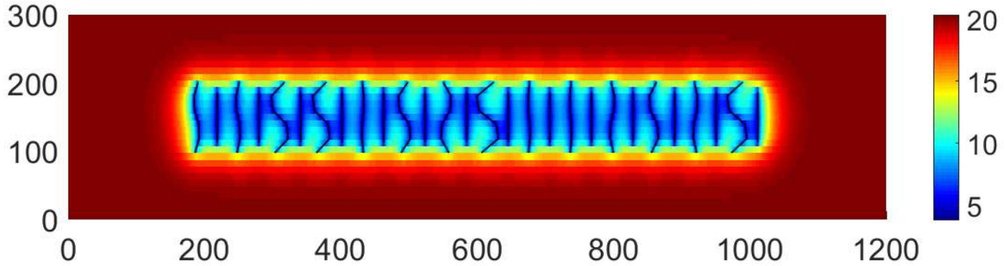

(a) Non-planar hydraulic fracture (Same total fracture length with Case 3)

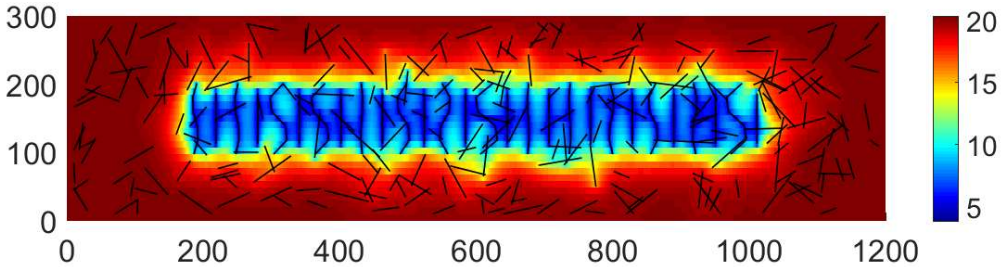

(b) Non-planar hydraulic fracture + natural fractures

Fig. 26 Pressure contour at the 3.75 years for Barnett shale reservoir with Non-planar fracture geometries and natural fractures (case 4)

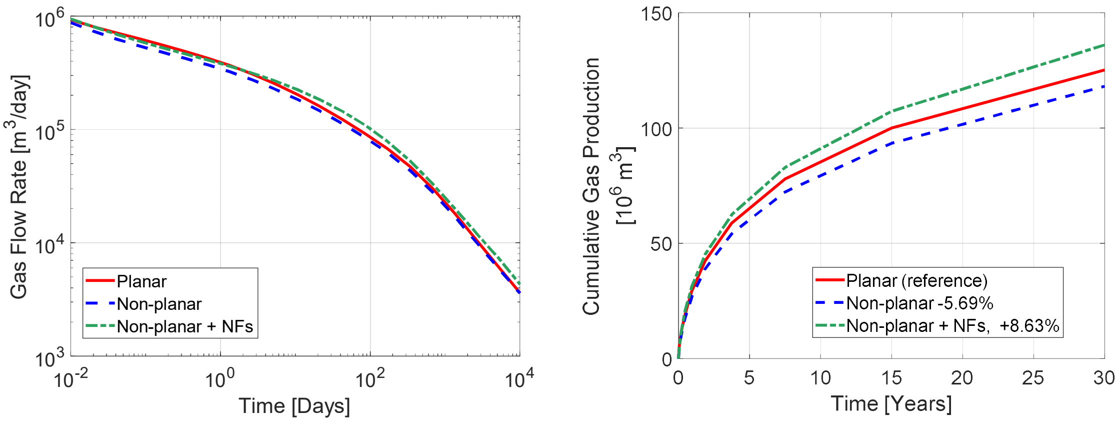

(a) (b)

Fig. 27 Comparison of gas flow rate (a) and cumulative production (b) between Planar, Non-planar and Non-planar & natural fractures cases

Firstly, the effect of complex fracture network on well performance is studied. **Fig 26** shows the pressure contour for the non-planar fractures with and without the natural fractures. Obviously, the case of natural fractures has larger and better stimulated reservoir volume (SRV). Thus, as shown in **Fig. 27**, the cumulative gas production of non-planar case with natural fracture has much higher value (14.56% improvements) than the planar case in the Case 3. While in the case of same total length, the non-planar fracture geometries will slightly degenerate the well performance (-5.69% reduction).

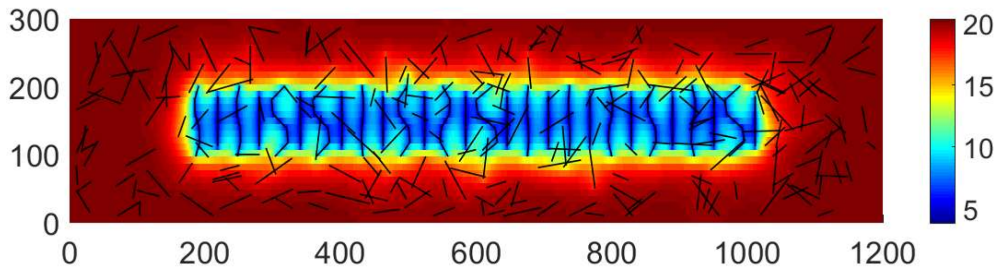

Non-planar hydraulic fracture + natural fractures + geomechanics effect

Fig. 28 Pressure contour at 3.75 years for Barnett shale reservoir with planar hydraulic fractures case and realistic case

The influence of geomechanics effect with fracture closure on well performance is further investigated by implementing Eqs. 15-17. **Fig. 28** shows the pressure contour at the 3.75 years for the planar case (Fig. 20a) and realistic case (Fig. 20b) with non-planar hydraulic fracture, natural fractures and geomechanics effect. As shown in **Fig. 29**, at the earlier production period**,** even realistic case has lower production than simple planar case due to geomechanics effect. But in the later production time, the contribution of natural fractures makes identical well performance between realistic case and simple planar case. Thus, the modeling of natural fractures and geomechanics effect is important for long-term production evaluation.

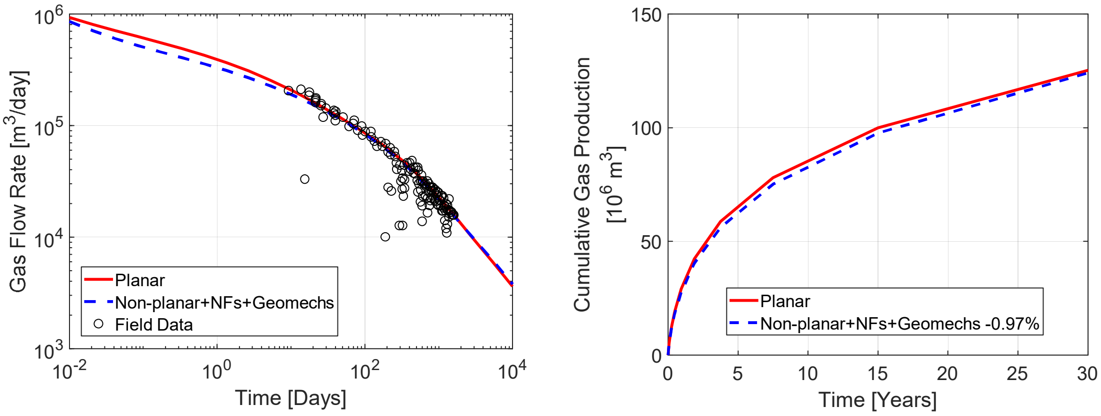

(a) (b)

Fig. 29 Comparison of gas flow rate (a) and cumulative production (b) between planar hydraulic fracture case and realistic case with non-planar, natural fractures and geomechanics effect

6 Conclusion

In this work, A generic numerical model and an open-source framework OpenShale are developed for shale gas simulation with state-of-art flow and storage mechanisms. It is verified against commercial and in-house reservoir simulators. The limitation of EDFM are also investigated quantality. Also, a field application of history matching and new model evaluation of geomechanics effect are successful performed. Several conclusions can be drawn as follows:

(1) A generic shale gas numerical model is developed which can be used to model any state-of-art storage and transport mechanisms, including gas adsorption, gas slippage & diffusion, non-Darcy flow as well as geomechanics effect by considering complex multi-scale fracture geometries.

(2) A general and open-source framework, OpenShale is developed and verified. With the help of the EDFM, Automatic Differentiation, and object-designed framework of OpenShale, one can easily use and extend OpenShale to simulate practical shale gas problem with arbitrary fracture geometries and new storage and transport mechanisms.

(3) EDFM can efficiently and accurately model irregular fracture geometry and complex fracture

networks. However, it cannot accurately model low-permeability fracture (error of 12.22%) and hydraulic fractures without help of LGR where have strong transient behavior and sharp gradient (error of 2.84%). Thus, projected EDFM and adaptively grid refinement will be implemented and tested in our future work.

(4) Shale gas transport and storage mechanisms, such as gas desorption and gas slippage &diffusion flow gas, are the most significant impact on well performance, follow by natural fractures, geomechanics effect and fracture geometry.

(5) OpenShale is capable of serving as an efficient, flexible research tool to evaluate new models with arbitrary non-linearity and fracture complexity. It can serve as a bridge between mechanism study and field scale engineering application.

Nomenclature

ρ_g = mass density of natural gas, kg/m^3
ϕ = absolute rock porosity, dimensionless
Ω_m = matrix domain
Ω_f = fracture domain
m_{ad} = storage mechanism term, kg/m^3
F_{app} = transport mechanism term, dimensionless
k_0 = absolute Darcy rock permeability, m^2
μ_g = viscosity of natural gas, Pa·s
p = pore pressure, Pa
q_w = volumetric sink/source term, m^3/day
b_g = inverse formation volume factor, dimensionless
M = molecular weight of natural gas, kg/mol
Z = compressibility factor of natural gas, dimensionless
R = ideal gas constant, 8.314 J/(mol·K)
T = reservoir temperature, K
T_{pr} = pseudo-temperature for natural gas, dimensionless
T_c = critical-temperature for natural gas, K
p_{pr} = pseudo-pressure for natural gas, dimensionless
p_c = critical-pressure for natural gas, Pa
$a_{0,1,2}$ = constants for Peng-Robinson equation of state, dimensionless
a,b = constants for Peng-Robinson equation of state, dimensionless
A,B = constants for Peng-Robinson equation of state, dimensionless
K,X,Y=constants for Lee-Conzalez-Eakin natural gas viscosity, dimensionless
ρ_s = mass density of bulk matrix, kg/m^3
ρ_{gsc} = mass density of natural gas at the standard condition, kg/m^3
V_L = Langmuir volume, m^3/kg

P_L = Langmuir pressure, Pa
V_m = BET volume, m^3/kg
P_s = BET pseudo-saturation pressure, Pa
p_r = psdueo-pressure for BET isotherm, dimensionless
C = constant for BET isotherm, dimensionless
n = constant for BET isotherm, dimensionless
α = rarefaction coefficient for gas slippage flow, dimensionless
K_n = Knudsen number, dimensionless
β = Darcy-Forchheimer coefficient, dimensionless
α_B = Biot's coefficient, dimensionless
P_c = reservoir confining overburden pressure, Pa
P_1 = reservoir effective stress when micro-fracture completely closed, Pa
m = constant for the Gangi's model, Pa
F_{cd} = fracture conductivity, md·ft
p_0 = initial reservoir pressure, m
σ = effective fracture closure stress, Pa
σ_{hf} = effective closure stress for hydraulic fracture, Pa
σ_{nf} = effective closure stress for natural fracture, Pa
σ_h = reservoir horizontal principle stress, Pa
σ_{hmin} = minimum reservoir horizontal principle stress, Pa
σ_{hmax} = maximum reservoir horizontal principle stress, Pa
k_f = absolute Darcy permeability of fracture, m^2
w_f = fracture width, m
V = bulk volume of a grid cell, m
δ = discrete domain delta function, dimensionless
Δt = solution time-step, day
$\psi_{f\text{-}m}$ = mass coupling term for matrix, dimensionless
$\psi_{m\text{-}f}$ = mass coupling term for fracture, dimensionless
p_{bh} = wellbore bottom hole pressure, Pa
k_{11} = absolute Darcy rock permeability in x-direction, m^2
k_{22} = absolute Darcy rock permeability in y-direction, m^2
r_e = equivalent radius for wellbore model, m
r_w = wellbore radius, m
s = wellbore skin factor, dimensionless
Δx = grid cell size in x-direction, m
Δy = grid cell size in y-direction, m
Δz = grid cell size in z-direction, m
WI = wellbore index, dimensionless
$\boldsymbol{x}$ = Unknown vector, -
$\boldsymbol{J}$ = Jacobian matrix, -
$\boldsymbol{R}$ = Residual vector, -
WI = wellbore index, dimensionless
p_f = pore pressure at the fracture domain, Pa
p_m = pore pressure at matrix domain, Pa

Preprints (www.preprints.org) | NOT PEER-REVIEWED | Posted: 9 January 2020 doi:10.20944/preprints202001.0080.v1

T = transmissibility, dimensionless
A = intersection area among fracture and matrix, m^2
d = average normal distance among fracture and matrix, m
h_f = length of a fracture cell, m
t = fracture transmissibility for fracture-fracture NNC, dimensionless

Subscripts:
NF = natural fracture
HF = hydraulic fracture
m = matrix
f = fracture
g = gas
w = well

References

Akkutlu, I.Y., Efendiev, Y., Vasilyeva, M. and Wang, Y., 2018. Multiscale model reduction for shale gas transport in poroelastic fractured media. Journal of Computational Physics, 353, pp.356-376.

Akkutlu IY, Fathi E. Multi-scale gas transport in shales with local kerogen heterogeneities. SPE J. 2012;17(4):1002–1011.

Alghalandis, Y.F., 2017. ADFNE: Open source software for discrete fracture network engineering, two and three dimensional applications. Computers & Geosciences, 102, pp.1-11.

Alramahi, B. and Sundberg, M.I., 2012, January. Proppant embedment and conductivity of hydraulic fractures in shales. In 46th US Rock Mechanics/Geomechanics Symposium. American Rock Mechanics Association.

Agarwal, R.G., 1979, January. " Real Gas Pseudo-Time"-A New Function For Pressure Buildup Analysis Of MHF Gas Wells. In SPE Annual Technical Conference and Exhibition. Society of Petroleum Engineers.

Bowker, K.A., 2007. Barnett shale gas production, Fort Worth Basin: Issues and discussion. AAPG bulletin, 91(4), pp.523-533.

Cipolla, C.L., Lolon, E.P., Erdle, J.C. and Rubin, B., 2010. Reservoir modeling in shale-gas reservoirs. SPE reservoir evaluation & engineering, 13(04), pp.638-653.

Cao, P., Liu, J. and Leong, Y.K., 2016. A fully coupled multiscale shale deformation-gas transport model for the evaluation of shale gas extraction. Fuel, 178, pp.103-117.

Civan F. Effective correlation of apparent gas permeability in tight porous media. Transp Porous Media. 2010;82(2):375–384.

Chen, Z., Liao, X., Zhao, X., Dou, X. and Zhu, L., 2015. Performance of horizontal wells with fracture networks in shale gas formation. Journal of Petroleum Science and Engineering, 133, pp.646-664.

Chen, Z., Liao, X., Zhao, X., Dou, X. and Zhu, L., 2016. A semi-analytical mathematical model for transient pressure behavior of multiple fractured vertical well in coal reservoirs incorporating with diffusion, adsorption, and stress-sensitivity. Journal of Natural Gas Science and Engineering, 29, pp.570-582.

Chen, Z., Liao, X., Sepehrnoori, K. and Yu, W., 2018. A Semianalytical Model for Pressure-Transient Analysis of Fractured Wells in Unconventional Plays With Arbitrarily Distributed Discrete Fractures. SPE Journal.
Chen Z, Liao X, Zhao X, Lyu S, Zhu L. A comprehensive productivity equation for multiple fractured vertical wells with non-linear effects under steady-state flow. J Pet Sci Eng. 2017; 149:9–24.
Civan F, Rai CS, Sondergeld CH. Shale-gas permeability and diffusivity inferred by improved formulation of relevant retention and transport mechanisms. Transp Porous Media. 2011;86(3):925–944.
Cinco, L., Samaniego, V. and Dominguez, A., 1978. Transient pressure behavior for a well with a finite-conductivity vertical fracture. Society of Petroleum Engineers Journal, 18(04), pp.253-264.
Elliott, J.R. and Lira, C.T., 2011. Introductory chemical engineering thermodynamics (Vol. 184). Upper Saddle River, NJ: Prentice Hall PTR.
Florence, F.A., Rushing, J., Newsham, K.E. and Blasingame, T.A., 2007, January. Improved permeability prediction relations for low permeability sands. In Rocky Mountain Oil & Gas Technology Symposium. Society of Petroleum Engineers.
Hoteit, H. and Firoozabadi, A., 2005. Multicomponent fluid flow by discontinuous Galerkin and mixed methods in unfractured and fractured media. Water Resources Research, 41(11).
Houze, O., Tauzin, E., Artus, V. and Larsen, L., 2010. The Analysis of Dynamic Data in Shale Gas Reservoirs–Part 1. company report, Kappa engineering, Houston, Texas, USA.
Gringarten, A.C., Ramey Jr, H.J. and Raghavan, R., 1974. Unsteady-state pressure distributions created by a well with a single infinite-conductivity vertical fracture. Society of Petroleum Engineers Journal, 14(04), pp.347-360.
Karimi-Fard, M., Durlofsky, L.J., Aziz, K., 2004. An efficient discrete-fracture model applicable for general purpose reservoir simulators. SPE J. 9 (2), 227e236.
Karimi-Fard, M., Gong, B. and Durlofsky, L.J., 2006. Generation of coarse - scale continuum flow models from detailed fracture characterizations. Water resources research, 42(10).
Karimi-Fard, M. and Durlofsky, L.J., 2016. A general gridding, discretization, and coarsening methodology for modeling flow in porous formations with discrete geological features. Advances in water resources, 96, pp.354-372.
Krogstad, S., Lie, K.A., Møyner, O., Nilsen, H.M., Raynaud, X. and Skaflestad, B., 2015, February. MRST-AD–an open-source framework for rapid prototyping and evaluation of reservoir simulation problems. In SPE reservoir simulation symposium. Society of Petroleum Engineers.
Gangi, A.F., 1978, October. Variation of whole and fractured porous rock permeability with confining pressure. In International Journal of Rock Mechanics and Mining Sciences & Geomechanics Abstracts (Vol. 15, No. 5, pp. 249-257). Pergamon.
Gensterblum, Y., Ghanizadeh, A., Cuss, R.J., Amann-Hildenbrand, A., Krooss, B.M., Clarkson, C.R., Harrington, J.F. and Zoback, M.D., 2015. Gas transport and storage capacity in shale gas reservoirs–A review. Part A: Transport processes. Journal of Unconventional Oil and Gas Resources, 12, pp.87-122.
Hajibeygi, H., Karvounis, D. and Jenny, P., 2011. A hierarchical fracture model for the iterative multiscale finite volume method. Journal of Computational Physics, 230(24), pp.8729-8743.

Hu, X., Wu, K., Li, G., Tang, J. and Shen, Z., 2018a. Effect of proppant addition schedule on the proppant distribution in a straight fracture for slickwater treatment. Journal of Petroleum Science and Engineering, 167, pp.110-119.
Hu, X., Wu, K., Song, X., Yu, W., Tang, J., Li, G. and Shen, Z., 2018b. A new model for simulating particle transport in a low‐viscosity fluid for fluid‐driven fracturing. AIChE Journal.
Javadpour F, Fisher D, Unsworth M. Nanoscale gas flow in shale gas sediments. J Can Pet Technol. 2007;46(10):55–61.
Jiang, J. and Younis, R.M., 2015. Numerical study of complex fracture geometries for unconventional gas reservoirs using a discrete fracture-matrix model. Journal of Natural Gas Science and Engineering, 26, pp.1174-1186.
Klinkenberg, L.J., 1941, January. The permeability of porous media to liquids and gases. In Drilling and production practice. American Petroleum Institute.
Lie, K.A., Krogstad, S., Ligaarden, I.S., Natvig, J.R., Nilsen, H.M. and Skaflestad, B., 2012. Open-source MATLAB implementation of consistent discretisations on complex grids. Computational Geosciences, 16(2), pp.297-322.
Li, Y., Zuo, L., Yu, W. and Chen, Y., 2018. A Fully Three Dimensional Semianalytical Model for Shale Gas Reservoirs with Hydraulic Fractures. Energies, 11(2), p.436.
Lee, S.H., Lough, M.F. and Jensen, C.L., 2001. Hierarchical modeling of flow in naturally fractured formations with multiple length scales. Water resources research, 37(3), pp.443-455.
Moinfar, A., Varavei, A., Sepehrnoori, K. et al. 2014. Development of an Efficient Embedded Discrete Fracture Model for 3D Compositional Reservoir Simulation in Fractured Reservoirs. SPE J. 19 (2): 289-303. SPE-154246-PA. http://dx.doi.org/10.2118/154246-PA.
Mahmoud, M., 2014. Development of a new correlation of gas compressibility factor (Z-factor) for high pressure gas reservoirs. Journal of Energy Resources Technology, 136(1), p.012903.
Olorode, O., Freeman, C.M., Moridis, G. and Blasingame, T.A., 2013. High-resolution numerical modeling of complex and irregular fracture patterns in shale-gas reservoirs and tight gas reservoirs. SPE Reservoir Evaluation & Engineering, 16(04), pp.443-455.
Olorode, O., Akkutlu, I.Y. and Efendiev, Y., 2017. Compositional Reservoir-Flow Simulation for Organic-Rich Gas Shale. SPE Journal.
Peaceman, D.W., 1983. Interpretation of well-block pressures in numerical reservoir simulation with nonsquare grid blocks and anisotropic permeability. Society of Petroleum Engineers Journal, 23(03), pp.531-543.
Rubin B. Accurate simulation of non-darcy flow in stimulated fractured shale reservoirs. In: SPE 132093, presented at the SPE western regional meeting, Anaheim, CA; May 27-29, 2010
Sakhaee-Pour A, Bryant SL. Gas permeability of shale. SPE Reservoir Eval Eng. 2012;15(4):401–409.
Sandve TH, Berre I, Nordbotten JM. An efficient multi-point flux approximation method for discrete fracture–matrix simulations. J Comput Phys. 2012;231(9):3784–3800
Ţene, M., Al Kobaisi, M.S. and Hajibeygi, H., 2016. Algebraic multiscale method for flow in heterogeneous porous media with embedded discrete fractures (F-AMS). Journal of Computational Physics, 321, pp.819-845.
Tan, L., Zuo, L. and Wang, B., 2018. Methods of decline curve analysis for shale gas reservoirs. Energies, 11(3), p.552.

Ţene, M., Bosma, S. B., Al Kobaisi, M. S., & Hajibeygi, H. (2017). Projection-based embedded discrete fracture model (pEDFM). Advances in Water Resources, 105, 205-216.

Wang FP, Reed RM. Pore networks and fluid flow in gas shales. In: SPE Annual Technical Conference and Exhibition. New Orleans, Louisiana, 2009.

Wang, K., Liu, H., Luo, J., Wu, K. and Chen, Z., 2017. A comprehensive model coupling embedded discrete fractures, multiple interacting continua, and geomechanics in shale gas reservoirs with multiscale fractures. Energy & Fuels, 31(8), pp.7758-7776.

Wasaki, A. and Akkutlu, I.Y., 2015. Permeability of organic-rich shale. SPE Journal, 20(06), pp.1-384.

Wu, W., Zhou, J., Kakkar, P., Russell, R. and Sharma, M.M., 2018. An Experimental Study on Conductivity of Unpropped Fractures in Preserved Shales. SPE Production & Operations.

Xu Y. Implementation and application of the Embedded Discrete Fracture Model (EDFM) for reservoir simulation in fractured reservoirs. Master Thesis, The University of Texas at Austin, 2015.

Xu, Y., Cavalcante Filho, J.S., Yu, W. and Sepehrnoori, K., 2017. Discrete-fracture modeling of complex hydraulic-fracture geometries in reservoir simulators. SPE Reservoir Evaluation & Engineering, 20(02), pp.403-422.

Yu, W., Xu, Y., Liu, M., Wu, K. and Sepehrnoori, K., 2018. Simulation of shale gas transport and production with complex fractures using embedded discrete fracture model. AIChE Journal, 64(6), pp.2251-2264.

Yu, W. and Sepehrnoori, K., 2014. Simulation of gas desorption and geomechanics effects for unconventional gas reservoirs. Fuel, 116, pp.455-464.

Yu, W., Sepehrnoori, K. and Patzek, T.W., 2016a. Modeling gas adsorption in Marcellus shale with Langmuir and bet isotherms. SPE Journal, 21(02), pp.589-600.

Yu, W., Wu, K., Zuo, L., Tan, X. and Weijermars, R., 2016b, August. Physical models for inter-well interference in shale reservoirs: relative impacts of fracture hits and matrix permeability. In Unconventional Resources Technology Conference, San Antonio, Texas, 1-3 August 2016 (pp. 1535-1558). Society of Exploration Geophysicists, American Association of Petroleum Geologists, Society of Petroleum Engineers.

Yu, W., Wu, K., Sepehrnoori, K. and Xu, W., 2017. A comprehensive model for simulation of gas transport in shale formation with complex hydraulic-fracture geometry. SPE Reservoir Evaluation & Engineering, 20(03), pp.547-561.

Yang*, R., Huang, Z., Li, G., Yu, W., Lashgari, H.R., Sepehrnoori, K. and Shen, Z., 2016a, August. A semianalytical method for modeling two-phase flow in coalbed methane reservoirs with complex fracture networks. In Unconventional Resources Technology Conference, San Antonio, Texas, 1-3 August 2016 (pp. 2387-2404). Society of Exploration Geophysicists, American Association of Petroleum Geologists, Society of Petroleum Engineers.

Yang R, Huang Z, Yu W, Li G, Ren W, Zuo L, Tan X, Sepehrnoori K, Tian S, Sheng M. A comprehensive model for real gas transport in shale formations with complex non-planar fracture networks. Sci Rep. 2016b; 6:36673.

Yang, R., Huang, Z., Li, G., Yu, W., Sepehrnoori, K., Lashgari, H.R., Tian, S., Song, X. and Sheng, M., 2017. A Semianalytical Approach to Model Two-Phase Flowback of Shale-Gas Wells with Complex-Fracture-Network Geometries. SPE Journal.

Zhang Y, Yu W, Sepehrnoori K, Di Y. A comprehensive numerical model for simulating fluid

 doi:10.20944/preprints202001.0080.v1

transport in nanopores. Sci Rep. 2017;7: 40507.

Zhou, Y., Tchelepi, H.A. and Mallison, B.T., 2011, January. Automatic differentiation framework for compositional simulation on unstructured grids with multi-point discretization schemes. In SPE Reservoir Simulation Symposium. Society of Petroleum Engineers.

Zuo, L., Yu, W. and Wu, K., 2016. A fractional decline curve analysis model for shale gas reservoirs. International Journal of Coal Geology, 163, pp.140-148.

Zeng, Z. and Grigg, R., 2006. A criterion for non-Darcy flow in porous media. Transport in porous media, 63(1), pp.57-69.